Free-Breathing Cardiac MR Stress Perfusion with Real-Time Slice Tracking

Tamer A. Basha[1], **Sébastien Roujol**[1], **Kraig V. Kissinger**[1], **Beth Goddu**[1], **Sophie Berg**[1], **Warren J. Manning**[1,2], and **Reza Nezafat**[1]

[1]Department of Medicine (Cardiovascular Division), Beth Israel Deaconess Medical Center and Harvard Medical School, Boston, MA

[2]Department of Radiology, Beth Israel Deaconess Medical Center and Harvard Medical School, Boston, MA

Abstract

Purpose—To develop a free-breathing cardiac MR perfusion sequence with slice tracking for use after physical exercise.

Methods—We propose to use a leading navigator, placed immediately before each 2D slice acquisition, for tracking the respiratory motion and updating the slice location in real-time. The proposed sequence was used to acquire CMR perfusion datasets in 12 healthy adult subjects and 8 patients. Images were compared with the conventional perfusion (i.e. without slice tracking) results from the same subjects. The location and geometry of the myocardium were quantitatively analyzed, and the perfusion signal curves were calculated from both sequences to show the efficacy of the proposed sequence.

Results—The proposed sequence was significantly better compared to the conventional perfusion sequence in terms of qualitative image scores. Changes in the myocardial location and geometry decreased by ~50% in the slice tracking sequence. Furthermore, the proposed sequence had signal curves that are smoother and less noisy.

Conclusion—The proposed sequence significantly reduces the effect of the respiratory motion on the image acquisition in both rest and stress perfusion scans.

Keywords

stress-perfusion; navigator; motion correction; real-time slice tracking; localized 2D restore pulses

Introduction

Cardiac magnetic resonance (CMR) perfusion allows assessment of the presence and extent of regional ischemia in patients with known or suspected coronary artery disease (CAD) (1–4). Studies comparing CMR perfusion vs. single photon emission computed tomography (SPECT) have demonstrated CMR perfusion to have superior diagnostic accuracy (5–7).

Correspondence to: Reza Nezafat, Ph.D., Beth Israel Deaconess Medical Center, 330 Brookline Ave, Boston, MA, 02215, Phone: 617-667-1747 ; Fax: 617-975-5480, rnezafat@bidmc.harvard.edu.

Data also show a correlation between CMR perfusion and fractional flow reserve, a physiological index of significant CAD (8–10). Clinically, ischemia is assessed *qualitatively* by identifying myocardial regions with delayed and reduced contrast uptake during stress. *Quantitative* CMR perfusion analysis enables absolute quantification of myocardial blood flow (MBF), which may improve the diagnostic accuracy of CMR perfusion, especially in multi-vessel CAD (11), and provide more observer-independent and reproducible results (12). Over the past decade, advances have been made to improve quantitative CMR perfusion including CMR acquisition methods (13–17), contrast infusion scheme (18–20), model-based quantification of MBF (21–23), and pixel-wise quantification (19,24). To extract the quantitative metrics from dynamic images, the image series should be aligned. However, this is difficult because of the breathing motion during the acquisition. Therefore, methods to reduce, or to compensate for, the respiratory motion effects are required.

To allow imaging with sufficient spatial and temporal resolution, parallel imaging (SENSE (25) or GRAPPA (26)) with an acceleration factor of 2 is often used. To further reduce the scan time, the redundancy of the data in spatio-temporal dimension can be exploited (27–29). *k-t* SENSE, *k-t* BLAST and *k-t* PCA methods can be used either to increase the in-plane spatial resolution (30–33), or to enable 3D perfusion (34,35) with acceleration rate as high as 12. CG-HYPR was recently proposed for perfusion imaging to increase both the number of slices and the spatial resolution (16). Studies also demonstrate the feasibility of compressed sensing and exploiting the sparsity in *k-t* dimension to achieve acceleration factor of 24 (36). However, acceleration methods based on spatio-temporal information are very sensitive to motion (37), with motion leading to deteriorating image quality. To mitigate this issue, *k-t* accelerated perfusion images are acquired during a prolonged breath-hold. However, not all patients are able to hold their breath during the scan, and there is commonly a respiratory drift that will impact the quality of the reconstruction (38,39).

Stress perfusion is commonly performed during pharmacological stress. However, MRI compatible treadmill and bicycle ergometers (40–42) have recently become available which enable perfusion imaging after physical stress (43,44). While pharmacologic stress has the advantage of uniformity in testing and a uniform vasodilator response, it provides no information regarding patient's exercise capacity and hemodynamic response to exercise (45,46). Despite the advantages, physical stress has several challenges related to the high heart rate, and rapid and deep breathing immediately after exercise. This constrains the choice of acceleration method, causes substantial through-plane and in-plane motion, and reduces the overall image quality. Therefore, improved motion correction is a necessity for perfusion after physical exercise in stress CMR.

Respiratory motion is often corrected *retrospectively* by registering images at different respiratory phases using different methods (47–49). While these methods can reduce the in-plane motion between different frames, through-plane motion is not compensated for. A respiratory navigator (NAV) positioned on the heart or on the right hemi-diaphragm (RHD), has been widely used in coronary MRI for *prospective* slice tracking (50–52). The imaging slice is adjusted in real-time to increase the acquisition efficiency and to partially compensate for respiratory motion (53). Slice tracking has also been used for imaging of the aortic valve (54), but little has been done for perfusion imaging. In a typical perfusion

sequence, a non-selective saturation pulse is applied with the image acquisition starting ~100 ms later to maximize the contrast. If the NAV pulse is applied immediately before the acquisition, the NAV signal will have a low signal-to-noise ratio (SNR) because of the preceding saturation pulse, and if the NAV is placed before the saturation pulse, there would be a relatively long delay between the NAV and the acquisition, reducing the accuracy of the slice tracking (55).

In this study, we sought to develop a free-breathing CMR perfusion sequence with real-time slice tracking to reduce the motion-induced mis-alignment between different frames and to reduce the through-plane motion. CMR perfusion images were acquired a) during normal breathing, b) during a simulated heavy breathing (i.e. increased respiratory rate and depth under instructions), and c) after physical supine ergometer exercise. Both quantitative and qualitative assessments of in-plane and through-plane motion were performed.

Methods

Pulse Sequence

Figure 1 shows the schematic of the proposed free-breathing CMR perfusion sequence with slice tracking. In this sequence, for each slice, a non-selective 90° saturation pulse is followed by a saturation delay of 100 ms, and then the acquisition is performed. For a prospective slice tracking, a NAV measurement is placed directly before the acquisition of each slice, and a NAV-restore pulse is applied immediately after each saturation pulse to locally restore the saturated magnetization in the RHD area for subsequent detection of the lung-liver interface of the NAV. For the NAV-restore pulse, we used a 2D spatially selective spiral pulse (56,57), with 16 spiral excitation turns in 10 msec, and a flip angle of −90° to restore the magnetization in a circular area centered on the RHD with a diameter of 50 mm. The NAV signal is then measured, using a 2D pencil beam NAV positioned on the RHD, centered at the same NAV-restore center point with a diameter of 30 mm, and immediately before starting each slice acquisition. The slice location is then prospectively changed in real-time using the RHD NAV signal with a constant superior-inferior scale factor of 0.6 (53,58). The time interval required for the restore pulse and navigator signal acquisition is calculated within the delay time between the saturation pulse and the data acquisition. The NAV signal is used only for tracking. No gating is performed (i.e. all data are accepted irrespective of the NAV location).

NAV-restore Validation

In order to validate the effect of the proposed NAV-restore pulse in a perfusion sequence, the pulse sequence was modified such that the NAV measurement was disabled, and the imaging pulses were applied exactly at the place of the NAV pulse. This sequence was then used to image an axial plane that passes through the RHD. Thus, the acquired image represents the NAV signal in the regular sequence.

We used this setup to acquire three images for the same axial slice: a) with no saturation pulse, no NAV-restore, b) with a saturation pulse but no NAV-restore, and c) with a saturation pulse, and NAV-restore.

Imaging Protocols

The CMR perfusion sequence with real-time slice tracking was implemented on a 1.5-T Philips Achieva (Philips Healthcare, Best, The Netherlands) system with a 32-channel cardiac phased-array receiver coil.

Twelve healthy adult subjects (6 females, 30.3±12.1 years) without any history of cardiovascular disease and eighteen patients (10 females, 52.5±15.1 years) referred for evaluation of cardiovascular disease were recruited. For this HIPAA-compliant study, the protocol was approved by our institutional review board, and written informed consent was obtained from all participants.

A bolus injection of 0.05 mmol/kg gadopentetate dimeglumine (Magnevist; Berlex Laboratories, Wayne, NY) was used, with 10 ml of saline after contrast, both at a rate of 4 ml/s.

Figure 2 shows the study design diagram with associated imaging protocol for each group. The proposed imaging sequence was evaluated in patients (group A, n=18) and healthy adult subjects undergoing heavy breathing (group B, n=8) or exercise stress perfusion (group C, n=3). While group A received only one contrast injection, group B and C received two separate injections with a time separation of 30–45 minutes to allow for contrast washout. In group A, the patients were randomized into two groups, one in which the rest perfusion was acquired without any NAV tracking (group A1, n=9), and the second with the proposed NAV tacking (group A2, n=9). In **group B**, each subject received two contrast injections (0.05 mmol/kg each). During one injection, the conventional perfusion sequence (i.e. without NAV tracking) was performed, but the NAV positions were also acquired during this scan. During the second injection, the proposed sequence with NAV slice tracking was performed. During both scans, the subject was instructed to take deep breaths at different rates and depth to simulate the maximum motion that we may encounter in patients after physical exercise. The order of the two perfusion scans was randomized. In **group C**, the perfusion protocols were performed directly after a supine bicycle stress (Figure 9.f), where the ergometer (Lode B.V., Groningen, NL), was mounted at the end of the MRI tabletop. After the initial imaging for scan prescription, the table was moved to outside of the scanner bore to perform exercise. An exercise protocol was performed with initial ergometer resistance of 25–50W (increase step=25W/2min, with ECG rhythm and blood pressure monitoring) to reach a target heart rate of ~140 bpm. The table was then positioned back into the magnet for post-exercise imaging. Similar to group B, each subject performed two exercises, each followed by a contrast injection of 0.05 mmol/kg and a perfusion scan, with a time separation of 30–45 minutes to allow for contrast washout. One perfusion scan was performed without NAV tracking, and the other scan was performed with NAV tracking. In the first scan of group C, it was observed that the navigator beam length was not sufficient for the large RHD motion after exercise (Figure 3). Thus, it was increased from 60 mm to 120 mm to accommodate the large RHD motion.

In all groups, the perfusion sequences were performed during free breathing. For CMR perfusion, a saturation-recovery steady-state free precession sequence (TR/TE = 2.5/1.27ms, flip angle = 50°, 90 frames, FOV = $320 \times 320 \text{mm}^2$, resolution = $2.7 \times 2.7 \times 10 \text{ mm}^3$, acquisition

matrix size = 120×120, SENSE factor=2, acquisition time = 150 ms/slice, saturation pulse delay = 100 ms, total imaging time = 175 ms/slice) was used to acquire 3 short-axis images per heart beat (base, mid, apex). In three cases (two stress and one rest exams), only two slices were acquired because of the higher heart rate (a maximum heart rate of 115 is allowed for the acquisition of three slices per cardiac cycle using this sequence).

Image and Statistical Analysis

All images and NAV measurements were exported into a separate PC station for quantitative analysis. All statistical analyses were performed using Matlab (v7.14, The MathWorks, Natick, MA) and SPSS (v20.0, SPSS Inc, Chicago, IL). Subjective image scores were used to evaluate the motion in the proposed sequence for all datasets in group A. A qualitative assessment of the amount of motion was performed by an experienced independent blinded reader with CMR perfusion imaging experience, using a four-point scale system: 0- non-diagnostic; 1- poor images quality due to motion artifacts; 2- good image quality but with mild motion artifacts; 3- excellent image quality with minimal motion artifacts. The signed rank test was used for imaging scores to test for the null hypothesis that the central tendency of the difference was zero for the NAV-tracking and non NAV-tracking images. A p value of <0.05 was considered to be significant.

Quantifications of Motion—The heavy breathing motion during imaging can result in both in-plane and through-plane motion. To quantitatively analyze these effects, we measured and quantified the changes in the center point and area of the left ventricle (LV) region in the resulting images as an indication of the effectiveness of the slice tracking.

In the perfusion sequence, each slice is imaged at exactly the same cardiac phase in all cardiac cycles, and thus the myocardium is expected to be located at the same position and have the same geometry and size in all time frames. If the breathing motion results in in-plane motion, we would expect this to reflect on the myocardial location in the image but not on its size or geometry since the same myocardium only moves to a different location within the same 2D slice. In contrast, if the breathing motion causes a shift in the acquired slice in the slice-selection direction, we would expect changes in the myocardial size and geometry. To capture these changes, we developed a software tool in Matlab to manually draw closed contours around the LV in all the acquired images (Figure 4.a). From these contours, the LV myocardial area and an approximate center point were estimated, using the center of mass method, in all slices and time frames (Figure 4.b).

Next, for each dataset, the distance between the estimated center points in each two successive time frames was calculated as a surrogate for the myocardial in-plane motion due to the breathing motion. Similarly, to address the effect of the through-plane motion, the difference in the myocardial area between each two successive time frames was calculated, where these changes were normalized with respect to the myocardial area at the contrast arrival dynamic. Then, both measurements (i.e. the center points changes and the normalized area changes) were compared between the NAV-tracking and non NAV-tracking sequences using a linear model analysis. In order to capture the measurements variability within and between-subject, the data from the NAV-tracking sequence for all subjects were structured

into one single vector with an indicator variable for time within subject. The data from the non NAV-tracking sequence were structured the same way. The overall slope between these two vectors, as well as the 95% confidence intervals, was computed taking into account the correlation of the measurements within each subject. The measurements were considered to be different if the confidence interval does not cover 1.0. The correlation (variance-covariance) structure was assumed to be compound symmetry which yielded the within and between-subject variance components which were used in the estimation of the difference and confidence interval via a linear mixed-effects model.

Next, to characterize the impact of the motion on the quantification of myocardial and blood signal changes in different time frames, the average intensity of the LV blood pool was calculated through different frames. To obtain these data, we used the same software tool described in the previous section to draw manual contours around the LV blood pool (Figure 4.a). For each slice, the signal curve was calculated using two methods: a) fixed-ROI method, where the contours drawn at the contrast arrival frame were propagated to all the other frames and use it to calculate the average intensity of the myocardium and blood pool, and b) tracked-ROI method, where contours were manually drawn in each dynamic to calculate the myocardium and blood-pool average intensity (Figure 4.c). Then, these curves were compared between free-breathing perfusion with and without NAV slice tracking in groups B and C.

Finally, the same intensity curves were calculated for the LV region, followed by the calculation of the upslope values in both NAV-tracking and non NAV-tracking sequences using the paired t-test, with a *p* value of <0.05 considered as significant.

Results

Figure 5 shows the effect of the saturation and NAV-restore pulses on the signal intensity level of the acquired NAV measurements. Figure 5.b shows the effect of the saturation pulse in reducing the signal intensity level while Figure 5.c shows the effect of the NAV-restore pulse to restore the signal intensity level in the NAV area to be almost similar to the standard one in Figure 5.a.

Based on the motion score system described above, qualitative image scores indicate that for group A (free breathing), the NAV-tracking images (3.2±0.6) were significantly better than the non NAV-tracking ones (2.6±1.2, *p* < 0.01). And for group B (deep and variable rate breathing) the NAV-tracking images (3.0±0.7) were significantly better than the non NAV-tracking ones (1.7±1.0, *p* < 0.01).

Figure 6 shows multiple frames from a representative slice in a subject from group B, who was instructed to take deep breaths at different rates and amounts to simulate the maximum motion that may be encountered in patients post-physical exercise, when no NAV slice tracking is used. Figure 7 shows multiple frames from the same slice and under the same breathing instructions but using the NAV slice tracking. Despite the heavy breathing pattern shown in the acquired navigator signal in Figure 7.f, the anatomical location of the myocardium was preserved through the different frames when using the NAV tracking. The

changes in the papillary muscle shape and myocardium were very small, indicating that the location of the acquired slice in the slice selection direction was not largely affected by the heavy breathing motion. Figure 8 shows another representative slice from a subject in group C, where the perfusion dataset was acquired after physical exercise and with NAV tracking. Despite the deep and high frequency breathing pattern shown in Figure 8.e, the anatomical features and geometry are well preserved through the different frames.

Table 1 summarizes the changes in the myocardial area and the location of the estimated myocardial center point throughout all the cases in groups B (deep and variable rate breathing) and C (bicycle stress), using the free-breathing perfusion with and without NAV tracking. The linear mixed model analysis led to overall slopes and corresponding confidence intervals of 1.64 ± 0.33 and 1.92 ± 0.24 for the myocardial center point motion in the readout and phase encoding directions respectively. Similarly, for the normalized area changes, the slope and the corresponding confidence interval from the analysis was 1.69 ± 0.21. Thus, the two sequences were significantly different in terms of the quantification of these cardiac indices.

The LV upslope for the non NAV-tracking was (4.3 ± 1.8 a.u.) and for the NAV-tracking was (4.5 ± 1.6 a.u.) with a *p* value of .36 for the rest cases, while for the stress cases, the LV upslope was (5.8 ± 1.1 a.u.) for the non NAV-tracking and (6.8 ± 1.6 a.u.) for the NAV-tracking with a *p* value < .05.

Figure 9 shows representative signal curves for two cases: one case from Group B (Figure 9.a and 9.c), where the subject was instructed to breathe heavily, and the other case from group C (Figure 9.b and 9.d) where the perfusion dataset was acquired after an actual physical exercise. In all graphs, the signal curves generated from the tracked-ROI method, shown in solid blue lines, are smooth and less noisy than the curves generated from the fixed-ROI method (dotted red lines). In each case, the signal curves, generated from the perfusion with slice tracking sequence, were smoother and less noisy than the ones generated without NAV slice tracking.

Discussion

In this study, we proposed and evaluated a novel free-breathing CMR perfusion sequence with real-time NAV slice tracking. The efficacy of the NAV slice tracking was demonstrated in free-breathing scans with and without heavy breathing, as well as after physical stress.

Using the NAV for slice tracking has always been a challenge in perfusion sequences due to the effect of the saturation pulse on the navigator signal. As an alternative solution, Pedersen et. al. proposed a calibrated motion model combined with a modified respiratory navigator to obtain a prospective slice tracking in perfusion imaging (59). In this work, the respiratory-induced heart motion is modeled through a pre-scan and the model is used to estimate the changes during the actual scan. However, this method requires the patient to have similar breathing pattern during the pre-scan and the actual perfusion scan. Therefore, such an

approach is not applicable for imaging after physical stress, where the rate and depth of the respiratory motion are changing as the patient recovers from the exercise.

In our sequence, we restore the RHD magnetization using a selective 2D restore pulse applied directly after the non-selective saturation pulse of the perfusion sequence. Therefore, the navigator measurement is not affected by the preceding saturation pulse. This navigator restore pulse is ~10 ms. So it can easily be placed during the saturation delay interval, which is ~100 ms, and thus does not affect the sequence timing. This method has a much simpler and practical setup (only conventional navigator setup is required) than using the calibrated motion model proposed in (59).

Although, the results from the quantification of the motion show residual motion, the amount is substantially smaller than free-breathing imaging without NAV tracking. Further, reduction of the motion may be achieved using image registration (47–49,60–64). We note that image registration cannot compensate for through-plane motion, therefore a combined approach can potentially reduce both in-plane and through-plane motion. We did not combine the proposed approach with image registration in this study, and the choice of the optimal registration algorithm remains to be studied and is beyond the scope of this study.

To improve the ability of the navigator for detecting large motion that occurs after exercise, we increased the navigator beam length to 120 mm from the 60 mm commonly used in coronary MRI (50–53). Except for this modification, we did not make any other modification in the implementation of the standard navigator acquisition or processing available in our imaging software. Thus, the proposed modification of the timing of the navigator can be easily adapted to the current navigator implementation.

Although the NAV tracking was used to correct for motion only in the head-foot direction, we found a significant reduction in the motion effect on the acquired short axis slices. This is likely because the motion in the head-foot direction is the most dominant motion component attributed to breathing, especially when imaging in the short-axis of the heart (58). The effect of RHD motion in the other two directions is minor, and could likely be corrected using image-based registration methods (48,64), but we did not investigate these correction methods in our study.

While the upslope measurements were not significantly different in images acquired with or without NAV tracking in the rest perfusion scans, the same measurements were different in images acquired immediately after physical exercise, presumably due to larger motion. We note that the number of subjects was limited, and further studies with a larger number of patients are needed to further validate the results from this pilot study. We also note that by using NAV tracking, we did not aim to improve the clinical efficacy of perfusion. Instead, our aim was to facilitate quantitative analysis by reducing the need for manual correction of motion between different phases.

We used a constant head-foot correction factor of 0.6 for NAV slice tracking (53,58,61). At rest, this factor is subject-specific (65), and may change after physical exercise. We did not systematically study the optimal tracking factor, but we expect the impact of small errors in tracking to be negligible. The proposed slice tracking will not compensate for respiratory or

cardiac motion that occurs during the data acquisition in each heart beat. Such motion will manifest itself as image blurring and artifacts rather than mis-registration between different frames.

In this study, we were not able to quantify myocardial perfusion because of the high contrast agent dose and lack of dual bolus or dual sequence acquisition. So, further studies are needed to address the impact of slice tracking on myocardial perfusion quantification. We also did not analyze the benefit of using a NAV for slice tracking in terms of reduction of analysis time for perfusion quantifications. It is expected that the NAV tracking would reduce or completely eliminate the need for manual registration between different frames but this was not studied and requires further investigation.

CMR imaging after physical stress is quite challenging and further improvements in imaging are still needed before routine clinical exams. As seen in this study, respiratory motion is one of the major limitations of acquiring clinically acceptable image quality after physical exercise. In addition, acquiring a reliable ECG could be challenging even at 1.5T. Presence of additional electronic equipment could interfere with ECG signal. In our experience, turning off the exercise equipment immediately after completion of the exercise is the most reliable approach to eliminate this source of interference. In addition, we have experienced issues with the moving ECG leads during the exercise, which could impact the subsequent perfusion scans. Rapid changes in heart rate also causes difficulties in performing an ECG gated scan, such as skipping heart beats, which could adversely impact the interpretation of the perfusion scans. Furthermore, coordination between the technologist(s) and the nurse(s) is essential to successfully perform the exercise and the subsequent rapid imaging.

Our study has several limitations. The number of subjects in each group was limited. We did not perform two different studies with days apart to assess the navigator efficiency between the two acquisitions. Perfusion imaging with slice tracking reduces the amount of motion, but does not totally eliminate it because of rapid motion and the inability of the navigator to accurately measure the heart motion. There were differences in the motion patterns between the two acquisitions that cannot be accounted for.

Conclusion

We demonstrate a free-breathing CMR perfusion sequence with RHD NAV slice tracking to reduce the impact of large respiratory motion we encounter in imaging after physical stress. The proposed slice tracking substantially reduces through-plane motion in CMR perfusion imaging and does not prolong the scan acquisition.

Acknowledgments

References

1. Nabi F, Malaty A, Shah DJ. Stress cardiac magnetic resonance. Curr Opin Cardiol. 2011; 26(5): 385–391. [PubMed: 21730829]

2. Klem I, Heitner JF, Shah DJ, Sketch MH Jr, Behar V, Weinsaft J, Cawley P, Parker M, Elliott M, Judd RM, Kim RJ. Improved detection of coronary artery disease by stress perfusion cardiovascular magnetic resonance with the use of delayed enhancement infarction imaging. J Am Coll Cardiol. 2006; 47(8):1630–1638. [PubMed: 16631001]

3. Nandalur KR, Dwamena BA, Choudhri AF, Nandalur MR, Carlos RC. Diagnostic performance of stress cardiac magnetic resonance imaging in the detection of coronary artery disease: A meta-analysis. J Am Coll Cardiol. 2007; 50(14):1343–1353. [PubMed: 17903634]

4. Jerosch-Herold M. Quantification of myocardial perfusion by cardiovascular magnetic resonance. J Cardiovasc Magn Reson. 2010; 12(1):57. [PubMed: 20932314]

5. Schwitter J, Nanz D, Kneifel S, Bertschinger K, Büchi M, Knüsel PR, Marincek B, Lüscher TF, von Schulthess GK. Assessment of myocardial perfusion in coronary artery disease by magnetic resonance: A comparison with positron emission tomography and coronary angiography. Circulation. 2001; 103(18):2230–2235. [PubMed: 11342469]

6. Greenwood JP, Maredia N, Younger JF, Brown JM, Nixon J, Everett CC, Bijsterveld P, Ridgway JP, Radjenovic A, Dickinson CJ, Ball SG, Plein S. Cardiovascular magnetic resonance and single-photon emission computed tomography for diagnosis of coronary heart disease (CE-MARC): a prospective trial. Lancet. 2011; 379(9814):453–460. [PubMed: 22196944]

7. Schwitter J, Wacker CM, van Rossum AC, Lombardi M, Al-Saadi N, Ahlstrom H, Dill T, Larsson HBW, Flamm SD, Marquardt M, Johansson L. MR-IMPACT: comparison of perfusion-cardiac magnetic resonance with single-photon emission computed tomography for the detection of coronary artery disease in a multicentre, multivendor, randomized trial. Eur Heart J. 2008; 29(4): 480–489. [PubMed: 18208849]

8. Rieber J, Huber A, Erhard I, Mueller S, Schweyer M, Koenig A, Schiele TM, Theisen K, Siebert U, Schoenberg SO, Reiser M, Klauss V. Cardiac magnetic resonance perfusion imaging for the functional assessment of coronary artery disease: a comparison with coronary angiography and fractional flow reserve. Eur Heart J. 2006; 27(12):1465–1471. [PubMed: 16720685]

9. Jogiya R, Kozerke S, Morton G, De Silva K, Redwood S, Perera D, Nagel E, Plein S. Validation of dynamic 3-dimensional whole heart magnetic resonance myocardial perfusion imaging against fractional flow reserve for the detection of significant coronary artery disease. J Am Coll Cardiol. 2012; 60(8):756–765. [PubMed: 22818072]

10. Manka R, Paetsch I, Kozerke S, Moccetti M, Hoffmann R, Schroeder J, Reith S, Schnackenburg B, Gaemperli O, Wissmann L. Whole-heart dynamic three-dimensional magnetic resonance perfusion imaging for the detection of coronary artery disease defined by fractional flow reserve: determination of volumetric myocardial ischaemic burden and coronary lesion location. Eur Heart J. 2012; 33(16):2016–2024. [PubMed: 22677136]

11. Patel AR, Antkowiak PF, Nandalur KR, West AM, Salerno M, Arora V, Christopher J, Epstein FH, Kramer CM. Assessment of advanced coronary artery disease: advantages of quantitative cardiac magnetic resonance perfusion analysis. J Am Coll Cardiol. 2010; 56(7):561–569. [PubMed: 20688211]

12. Chih S, Macdonald P, Feneley M, Law M, Graham R, McCrohon J. Reproducibility of adenosine stress cardiovascular magnetic resonance in multi-vessel symptomatic coronary artery disease. J Cardiovasc Magn Reson. 2010; 12(1):42. [PubMed: 20663155]

13. Kim D, Axel L. Multislice, dual-imaging sequence for increasing the dynamic range of the contrast-enhanced blood signal and CNR of myocardial enhancement at 3T. J Magn Reson Imaging. 2005; 23(1):81–86. [PubMed: 16331593]

14. Wang Y, Moin K, Akinboboye O, Reichek N. Myocardial first pass perfusion: Steady-state free precession versus spoiled gradient echo and segmented echo planar imaging. Magn Reson Med. 2005; 54(5):1123–1129. [PubMed: 16217785]

15. Adluru G, McGann C, Speier P, Kholmovski EG, Shaaban A, DiBella EV. Acquisition and reconstruction of undersampled radial data for myocardial perfusion magnetic resonance imaging. J Magn Reson Imaging. 2009; 29(2):466–473. [PubMed: 19161204]

16. Ge L, Kino A, Griswold M, Mistretta C, Carr JC, Li D. Myocardial perfusion MRI with sliding window conjugate gradient HYPR. Magn Reson Med. 2009; 62(4):835–839. [PubMed: 19672941]

17. Salerno M, Sica CT, Kramer CM, Meyer CH. Optimization of spiral-based pulse sequences for first-pass myocardial perfusion imaging. Magn Reson Med. 2011; 65(6):1602–1610. [PubMed: 21590802]

18. Utz W, Niendorf T, Wassmuth R, Messroghli D, Dietz R, Schulz-Menger J. Contrast–dose relation in first-pass myocardial MR perfusion imaging. J Magn Reson Imaging. 2007; 25(6):1131–1135. [PubMed: 17520736]

19. Christian TF, Rettmann DW, Aletras AH, Liao SL, Taylor JL, Balaban RS, Arai AE. Absolute myocardial perfusion in canines measured by using dual-bolus first-pass MR imaging. Radiology. 2004; 232(3):677–684. [PubMed: 15284436]

20. Köstler H, Ritter C, Lipp M, Beer M, Hahn D, Sandstede J. Comparison of different contrast agents and doses for quantitative MR myocardial perfusion imaging. J Magn Reson Imaging. 2008; 28(2):382–389. [PubMed: 18666144]

21. Kroll K, Wilke N, Jerosch-Herold M, Wang Y, Zhang Y, Bache R, Bassingthwaighte J. Modeling regional myocardial flows from residue functions of an intravascular indicator. Am Physiol-Heart C. 1996; 271(4):H1643–H1655.

22. Jerosch-Herold M, Wilke N, Wang Y, Gong G-R, Mansoor AM, Huang H, Gurchumelidze S, Stillman AE. Direct comparison of an intravascular and an extracellular contrast agent for quantification of myocardial perfusion. Int J Cardiac Imag. 1999; 15(6):453–464.

23. Ishida M, Ichihara T, Nagata M, Ishida N, Takase S, Kurita T, Ito M, Takeda K, Sakuma H. Quantification of myocardial blood flow using model based analysis of first-pass perfusion MRI: Extraction fraction of Gd-DTPA varies with myocardial blood flow in human myocardium. Magn Reson Med. 2011; 66(5):1391–1399. [PubMed: 21469192]

24. Hsu L-Y, Groves DW, Aletras AH, Kellman P, Arai AE. A quantitative pixel-wise measurement of myocardial blood flow by contrast-enhanced first-pass CMR perfusion imaging: microsphere validation in dogs and feasibility study in humans. JACC: Cardiovascular Imaging. 2012; 5(2): 154–166. [PubMed: 22340821]

25. Pruessmann KP, Weiger M, Scheidegger MB, Boesiger P. SENSE: sensitivity encoding for fast MRI. Magn Reson Med. 1999; 42(5):952–962. [PubMed: 10542355]

26. Griswold MA, Jakob PM, Heidemann RM, Nittka M, Jellus V, Wang J, Kiefer B, Haase A. Generalized autocalibrating partially parallel acquisitions (GRAPPA). Magn Reson Med. 2002; 47(6):1202–1210. [PubMed: 12111967]

27. Kellman P, Derbyshire JA, Agyeman KO, McVeigh ER, Arai AE. Extended coverage first-pass perfusion imaging using slice-interleaved TSENSE. Magn Reson Med. 2004; 51(1):200–204. [PubMed: 14705062]

28. Tsao J, Boesiger P, Pruessmann KP. *k-t* BLAST and *k-t* SENSE: dynamic MRI with high frame rate exploiting spatiotemporal correlations. Magn Reson Med. 2003; 50(5):1031–1042. [PubMed: 14587014]

29. Jahnke C, Paetsch I, Gebker R, Bornstedt A, Fleck E, Nagel E. Accelerated 4D Dobutamine stress MR imaging with *k-t* BLAST: feasibility and diagnostic performance. Radiology. 2006; 241(3): 718–728. [PubMed: 17065561]

30. Plein S, Ryf S, Schwitter J, Radjenovic A, Boesiger P, Kozerke S. Dynamic contrast-enhanced myocardial perfusion MRI accelerated with *k-t* SENSE. Magn Reson Med. 2007; 58(4):777–785. [PubMed: 17899611]

31. Gebker R, Jahnke C, Paetsch I, Schnackenburg B, Kozerke S, Bornstedt A, Fleck E, Nagel E. MR Myocardial perfusion imaging with *k*-space and time broad-use linear acquisition speed-up technique: feasibility study. Radiology. 2007; 245(3):863–871. [PubMed: 18024455]

32. Plein S, Kozerke S, Suerder D, Luescher TF, Greenwood JP, Boesiger P, Schwitter J. High spatial resolution myocardial perfusion cardiac magnetic resonance for the detection of coronary artery disease. Eur Heart J. 2008; 29(17):2148–2155. [PubMed: 18641047]

33. Gebker R, Jahnke C, Manka R, Frick M, Hucko T, Kozerke S, Schnackenburg B, Fleck E, Paetsch I. High spatial resolution myocardial perfusion imaging during high dose dobutamine/atropine stress magnetic resonance using *k-t* SENSE. Int J Cardiol. 2011; 158(3):411–416. [PubMed: 21345497]

34. Vitanis V, Manka R, Giese D, Pedersen H, Plein S, Boesiger P, Kozerke S. High resolution three dimensional cardiac perfusion imaging using compartment based *k-t* principal component analysis. Magn Reson Med. 2011; 65(2):575–587. [PubMed: 20928876]

35. Shin T, Nayak KS, Santos JM, Nishimura DG, Hu BS, McConnell MV. Three-dimensional first-pass myocardial perfusion MRI using a stack-of-spirals acquisition. Magn Reson Med. 2012; 69(3):839–844. [PubMed: 22556062]

36. Feng, L.; Xu, J.; Kim, D.; Axel, L.; Sodickson, D.; Otazo, R. Combination of compressed sensing, parallel imaging and partial Fourier for highly-accelerated 3D first-pass cardiac perfusion. Proceedings of the 19th Scientific Meeting of ISMRM; 2011. p. 4368

37. Tsao J, Kozerke S. MRI temporal acceleration techniques. J Magn Reson Imaging. 2012; 36(3):543–560. [PubMed: 22903655]

38. Pennell DJ, Underwood SR, Manzara CC, Swanton RH, Walker JM, Ell PJ, Longmore DB. Magnetic resonance imaging during dobutamine stress in coronary artery disease. Am J Cardiol. 1992; 70(1):34–40. [PubMed: 1615867]

39. Dakik HA, Vempathy H, Verani MS. Tolerance, hemodynamic changes, and safety of dobutamine stress perfusion imaging. J Nucl Cardiol. 1996; 3(5):410–414. [PubMed: 8902673]

40. Foster EL, Arnold JW, Jekic M, Bender JA, Balasubramanian V, Thavendiranathan P, Dickerson JA, Raman SV, Simonetti OP. MR-compatible treadmill for exercise stress cardiac magnetic resonance imaging. Magn Reson Med. 2012; 67(3):880–889. [PubMed: 22190228]

41. Jeneson JAL, Schmitz JPJ, Hilbers PAJ, Nicolay K. An MR-compatible bicycle ergometer for in-magnet whole-body human exercise testing. Magn Reson Med. 2010; 63(1):257–261. [PubMed: 19918886]

42. Gusso S, Salvador C, Hofman P, Cutfield W, Baldi J, Taberner A, Nielsen P. Design and testing of an MRI-compatible cycle ergometer for non-invasive cardiac assessments during exercise. Biomed Eng Online. 2012; 11(1):13. [PubMed: 22423637]

43. Thavendiranathan P, Dickerson J, Scandling D, Balasubramanian V, Hall N, Foster E, Arnold J, Pennell M, Simonetti O, Raman S. Myocardial function and perfusion assessment with exercise stress cardiovascular magnetic resonance using an MRI-compatible treadmill in patients referred for stress SPECT. J Cardiovasc Magn Reson. 2012; 14(Suppl 1):1. [PubMed: 22226320]

44. Greulich S, Bruder O, Parker M, Schumm J, Grun S, Schneider S, Klem I, Sechtem U, Mahrholdt H. Comparison of exercise electrocardiography and stress perfusion CMR for the detection of coronary artery disease in women. J Cardiovasc Magn Reson. 2012; 14(1):36. [PubMed: 22697372]

45. Alexander KP, Shaw LJ, DeLong ER, Mark DB, Peterson ED. Value of exercise treadmill testing in women. J Am Coll Cardiol. 1998; 32(6):1657–1664. [PubMed: 9822093]

46. Mark DB, Hlatky MA, Harrell JFE, Lee KL, Califf RM, Pryor DB. Exercise treadmill score for predicting prognosis in coronary artery disease. Ann Intern Med. 1987; 106(6):793–800. [PubMed: 3579066]

47. Bidaut LM, Vallée J-P. Automated registration of dynamic MR images for the quantification of myocardial perfusion. J Magn Reson Imaging. 2001; 13(4):648–655. [PubMed: 11276113]

48. Dornier C, Ivancevic MK, Thévenaz P, Vallée J-P. Improvement in the quantification of myocardial perfusion using an automatic spline-based registration algorithm. J Magn Reson Imaging. 2003; 18(2):160–168. [PubMed: 12884327]

49. Adluru G, DiBella EVR, Schabel MC. Model-based registration for dynamic cardiac perfusion MRI. J Magn Reson Imaging. 2006; 24(5):1062–1070. [PubMed: 17031818]

50. Sachs TS, Meyer CH, Hu BS, Kohli J, Nishimura DG, Macovski A. Real-time motion detection in spiral MRI using navigators. Magn Reson Med. 1994; 32(5):639–645. [PubMed: 7808265]

51. Oshinski JN, Hofland L, Mukundan S, Dixon WT, Parks WJ, Pettigrew RI. Two-dimensional coronary MR angiography without breath holding. Radiology. 1996; 201(3):737–743. [PubMed: 8939224]

52. Stuber M, Botnar RM, Danias PG, Sodickson DK, Kissinger KV, Van Cauteren M, De Becker J, Manning WJ. Double-oblique free-breathing high resolution three-dimensional coronary magnetic resonance angiography. J Am Coll Cardiol. 1999; 34(2):524–531. [PubMed: 10440168]

53. Danias PG, McConnell MV, Khasgiwala VC, Chuang ML, Edelman RR, Manning WJ. Prospective navigator correction of image position for coronary MR angiography. Radiology. 1997; 203(3):733–736. [PubMed: 9169696]

54. Kozerke S, Hasenkam JM, Nygaard H, Paulsen PK, Pedersen EM, Boesiger P. Heart motion-adapted MR velocity mapping of blood velocity distribution downstream of aortic valve prostheses: initial experience. Radiology. 2001; 218(2):548–555. [PubMed: 11161177]

55. Spuentrup E, Manning WJ, Botnar RM, Kissinger KV, Stuber M. Impact of navigator timing on free-breathing submillimeter 3D coronary magnetic resonance angiography. Magn Reson Med. 2002; 47(1):196–201. [PubMed: 11754460]

56. Pauly J, Nishimura D, Macovski A. A k-space analysis of small-tip-angle excitation. J Magn Reson. 1989; 81(1):43–56.

57. Hardy CJ, Cline HE. Broadband nuclear magnetic resonance pulses with two-dimensional spatial selectivity. J Appl Phys. 1989; 66(4):1513–1516.

58. Wang Y, Riederer SJ, Ehman RL. Respiratory motion of the heart: kinematics and the implications for the spatial resolution in coronary imaging. Magn Reson Med. 1995; 33(5):713–719. [PubMed: 7596276]

59. Pedersen H, Kelle S, Ringgaard S, Schnackenburg B, Nagel E, Nehrke K, Kim WY. Quantification of myocardial perfusion using free-breathing MRI and prospective slice tracking. Magn Reson Med. 2009; 61(3):734–738. [PubMed: 19097242]

60. Wong KK, Yang ES, Wu EX, Tse H-F, Wong ST. First-pass myocardial perfusion image registration by maximization of normalized mutual information. J Magn Reson Imaging. 2008; 27(3):529–537. [PubMed: 18183575]

61. Gupta V, Hendriks EA, Milles J, van der Geest RJ, Jerosch-Herold M, Reiber JHC, Lelieveldt BPF. Fully automatic registration and segmentation of first-pass myocardial perfusion MR image sequences. Acad Radiol. 2010; 17(11):1375–1385. [PubMed: 20801696]

62. Wollny, G.; Kellman, P.; Santos, A.; Ledesma, M-J. Nonrigid Motion Compensation of Free Breathing Acquired Myocardial Perfusion Data. In: Handels, H.; Ehrhardt, J.; Deserno, TM.; Meinzer, H-P.; Tolxdorff, T., editors. Bildverarbeitung für die Medizin 2011, Informatik aktuell. Springer; Berlin Heidelberg: 2011. p. 84-88.

63. Milles, J.; Geest, RJ.; Jerosch-Herold, M.; Reiber, JHC.; Lelieveldt, BPF. Fully automated registration of first-pass myocardial perfusion MRI using independent component analysis. In: Karssemeijer, N.; Lelieveldt, B., editors. Information Processing in Medical Imaging. Volume 4584, Lecture Notes in Computer Science. Springer; Berlin Heidelberg: 2007. p. 544-555.

64. Wollny G, Kellman P, Santos A, Ledesma-Carbayo MJ. Automatic motion compensation of free breathing acquired myocardial perfusion data by using independent component analysis. Med Image Anal. 2012; 16(5):1015–1028. [PubMed: 22465078]

65. Moghari MH, Hu P, Kissinger KV, Goddu B, Goepfert L, Ngo L, Manning WJ, Nezafat R. Subject-specific estimation of respiratory navigator tracking factor for free-breathing cardiovascular MR. Magn Reson Med. 2011; 67(6):1665–1672. [PubMed: 22134885]
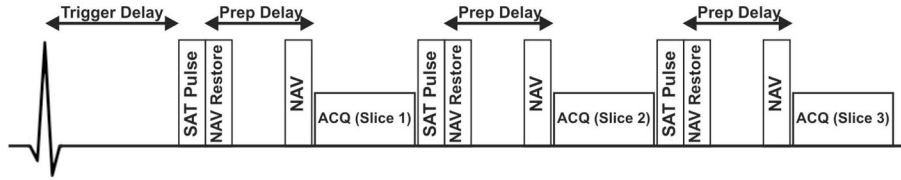
Figure 1.
Pulse sequence diagram for the proposed multi-slice free-breathing CMR perfusion sequence with real-time navigator (NAV) slice tracking using the 2D-pencil beam navigator with a restore pulse. Immediately after the non-selective saturation pulse (SAT Pulse), a 2D selective NAV restore pulse (−90°) is applied. This allows restoration of the liver signal that can be used to monitor the respiratory motion. A 2D pencil beam NAV signal is subsequently acquired prior to the image acquisition (ACQ) and used for adjusting the imaging position using a simple tracking factor of 0.6. The NAV is used only for slice tracking and not for gating. Therefore all data are accepted.
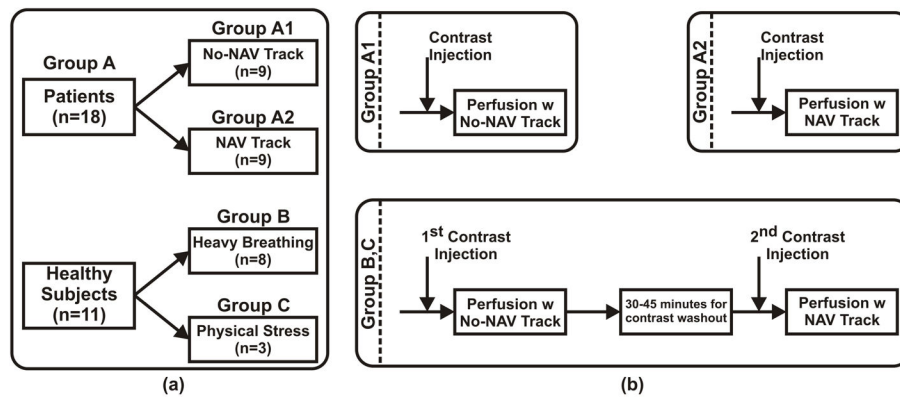
Figure 2.
Study design. a) Volunteers are divided into three groups: group A includes the patients, group B includes healthy adult subjects, that were instructed to breath heavily during imaging, and group C includes healthy subjects, who underwent a physical stress directly before imaging. b) The imaging protocol for each group.
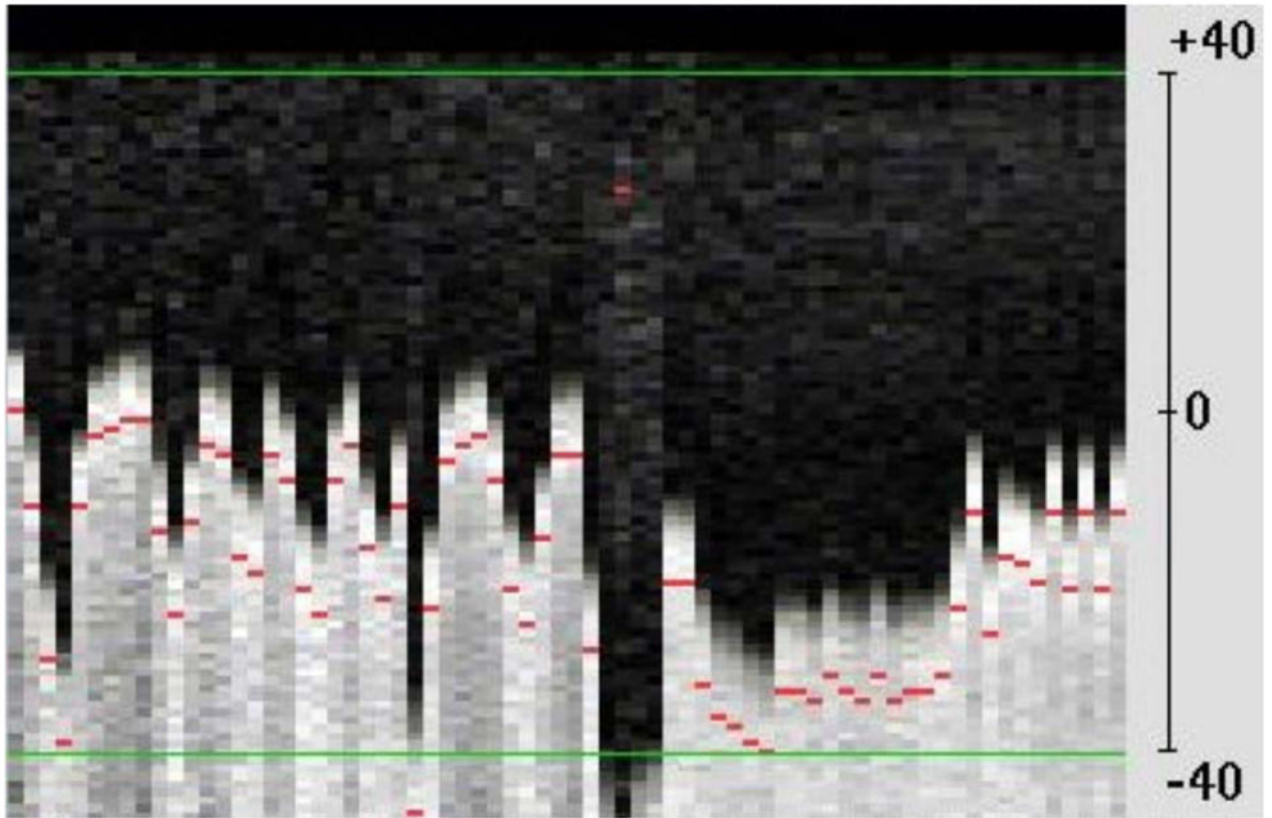
Figure 3.
An example of failing navigator tracking because of the small beam length used in this scan (80 mm). In all stress scans, the beam navigator length was increased to 120 mm to accommodate for the large RHD motion after exercise.
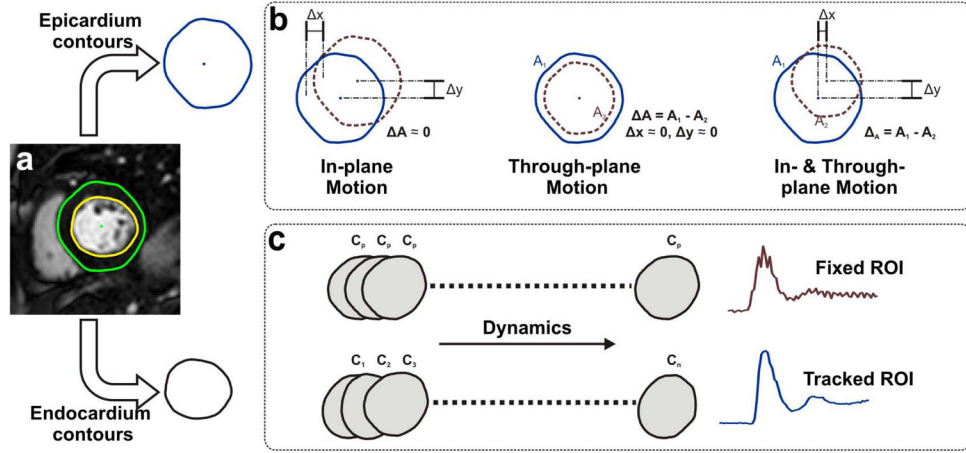
Figure 4.
A schematic of the image analysis to quantify the motion effect in perfusion images. (a) Epicardium and endocardium contours are drawn on all the slices, (b) For each epicardium contour, the area is calculated and an approximate center point is estimated. Then, differences in area and center point location are calculated between each two successive time frames. If the breathing motion results in in-plane motion, we expect to see a shift in the center point but not the area. However, if it results in through-plane motion, we expect to see a different area, because a different slice was imaged, (c) The drawn endocardium contours are used to calculate the signal curves in two methods: 1) fixed-ROI, where the contour drawn at the contrast arrival point is propagated through all frames and the average intensity is calculated from the images; and 2) tracked-ROI, where the average intensity is calculated in each dynamic slice using the contour that was drawn specifically for that dynamic.
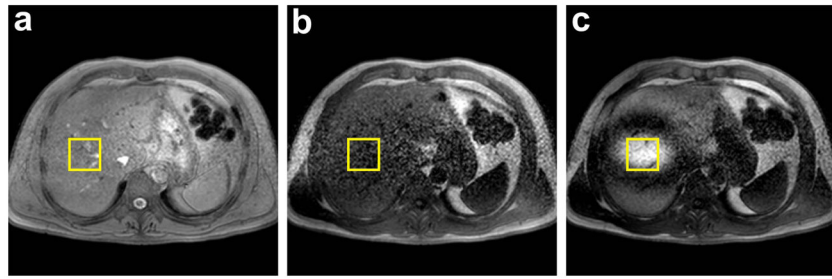
Figure 5.
The effect of saturation and NAV-restore pulses on the NAV measurements. a) Neither saturation nor NAV-restore pulses are applied (i.e. similar to most of the regular sequences), b) Non-selective saturation pulse is applied without a NAV-restore, and c) a spatially selective NAV-restore pulse is applied after the saturation pulse.
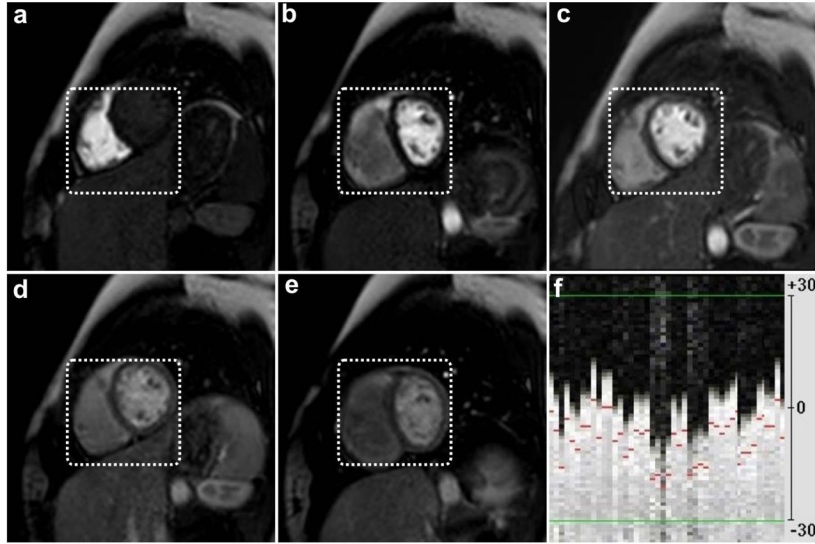
Figure 6.
(a–e) Selected frames for a representative short-axis slice from a 20 year old healthy subject instructed to breathe heavily to simulate the breathing pattern after a physical exercise. f) the corresponding navigator signal, in mm, acquired immediately prior to the slice acquisition. However, the NAV measurements were not used for any slice tracking. A white dotted fixed box is placed around the myocardium at the contrast arrival dynamic (dynamic b), and then propagated through the other frames to emphasize the myocardial in-plane motion. For the through-plane motion, note the changes in the heart and liver locations through frames due to the heavy breathing motion.
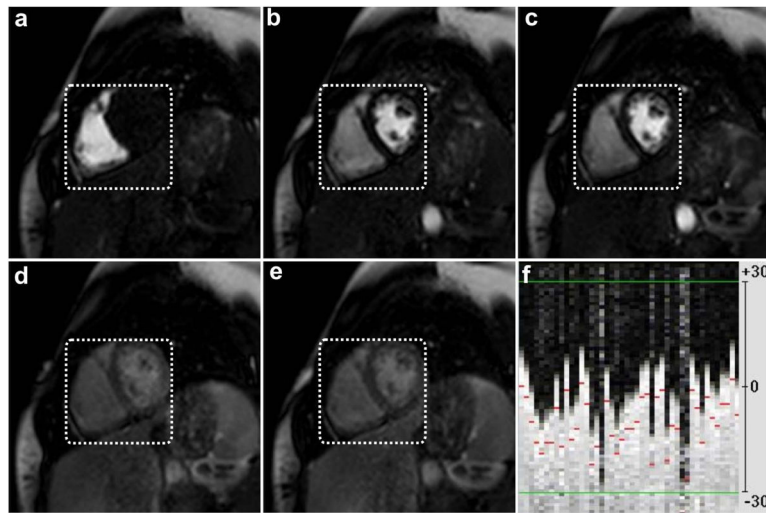
Figure 7.
(a–e) Selected frames for the same short-axis slice in Figure 6, acquired under the same breathing instruction but using the NAV slice tracking, f) the corresponding navigator signal, in mm, acquired immediately prior to the slice acquisition, which shows substantial respiratory motion during imaging. The same fixed box in Figure 6 is used to emphasize the reduction in the myocardial in-plane motion. Note the good depiction and preservation of the anatomical location during different frames.
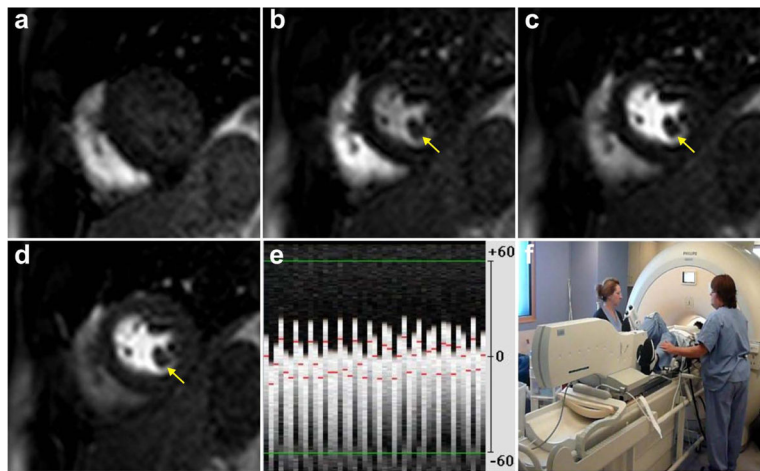
Figure 8.
(a–d) Selected frames from a representative short-axis slice post physical exercise, e) the corresponding navigator signal, in mm, which shows rapid deep breathing by the subject, and f) the physical stress setup used during the study. Note that the anatomical features and geometry are well preserved in different frames (see arrows) even in the presence of deep and fast breathing after physical exercise. The maximal RHD NAV displacement was 18mm.
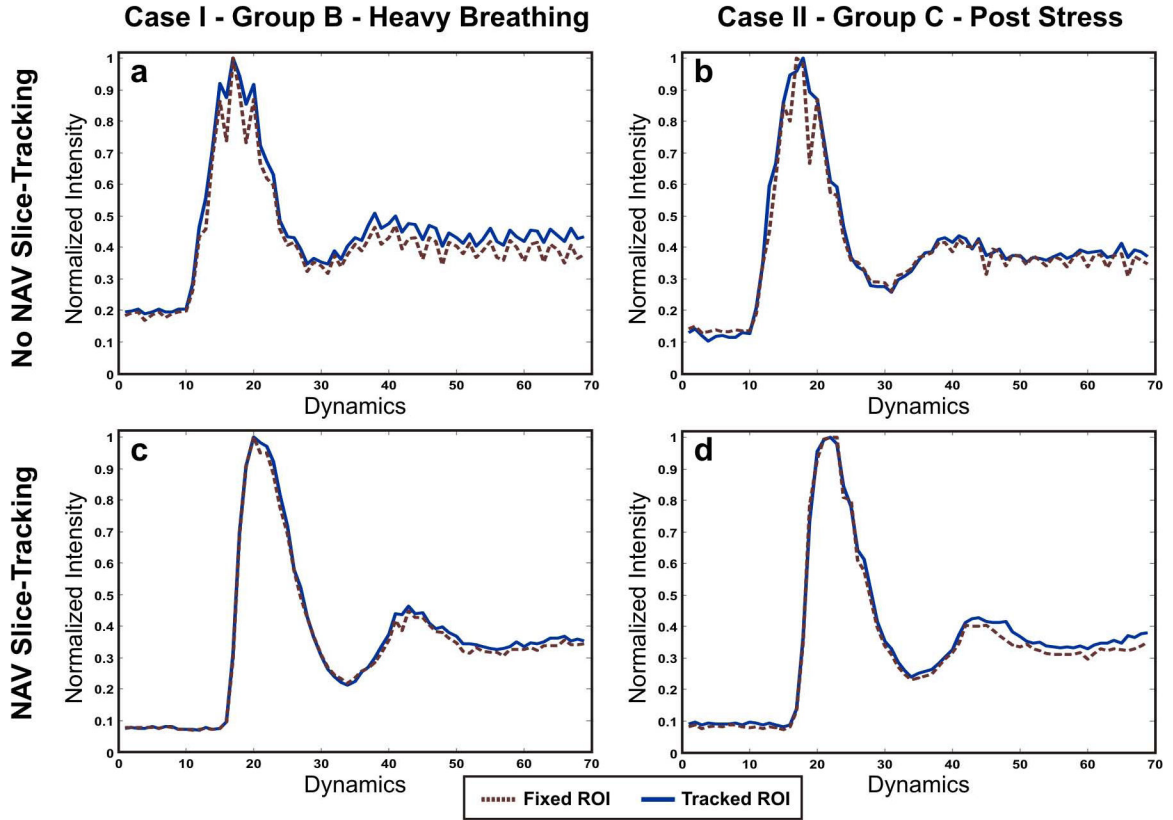
Figure 9.
Normalized signal intensity curves from two cases: one case from Group B (first column; graph a and c) and one case from Group C (second column; graphs b and d). In each case, the upper row shows the curve calculated from the non NAV-tracking perfusion sequence, and the lower row shows the curve calculated from the NAV-tracking perfusion sequence. In each graph, the perfusion curve is calculated using two methods: fixed-ROI (in red dotted lines), and manually tracked-ROI (in solid blue lines). Note that in general, the manually tracked ROIs result in smoother curves. However, when using the NAV slice tracking, the curves becomes smoother for both fixed and manually tracked ROIs.

Table 1

Mean square (MSE), and standard deviation (STD) of the calculated changes in the normalized myocardial area and the estimated myocardial center point throughout different time frames and slices from groups B and C. While the effect of the breathing motion is more apparent on the phase encoding direction, reflected on the center point location changes in both readout and phase encoding directions, the proposed sequence has reduced the center point motion average and standard deviation by almost half.

	Area (%)	Motion of Myocardial Center Point	
		Readout Direction (mm)	Phase Encoding (mm)
No NAV Tracking	8.9±11.2	4.1±5.0	9.3±11.0
NAV Tracking	5.4±6.5	2.9±3.6	4.9±5.8